Q-Mamba: Towards more efficient Mamba models via post-training quantization

Tianqi Chen[1,2] *, **Yuanteng Chen**[1,2] *, **Peisong Wang**[1,2,3], **Weixiang Xu**[1], **Zeyu Zhu**[1], **Jian Cheng**[1,2,3,4†]
[1] C[2]DL, Institute of Automation, Chinese Academy of Sciences
[2]School of Artificial Intelligence, University of Chinese Academy of Sciences
[3]AIRIA [4]Maicro.ai
{chentianqi2023,chenyuanteng2024,xuweixiang2018,zhuzeyu2021}@ia.ac.cn,
{peisong.wang,jcheng}@nlpr.ia.ac.cn

Abstract

State Space Models (SSMs), such as Mamba, have recently demonstrated potential in language understanding tasks, positioning them as competitors to transformer architectures. However, our investigations reveal that the Mamba architecture still has room for further optimization—not only in linear projections but also in state caches, which contribute significantly to memory consumption, particularly after quantizing the former into low bits. After a theoretical analysis of the causes of outliers in states, we propose **Decoupled Scale Quantization (DSQ)**, which mitigates outliers in both the state and channel dimensions by applying separate quantization scales. To preserve the selective ability of quantized Mamba, we introduce **Efficient Selectivity Reconstruction (ESR)**, a novel quantization simulation scheme in block-wise reconstruction that enables fast parallel scan algorithms with the non-linear quantization function. We demonstrate the effectiveness of Q-Mamba across various quantization settings, model sizes, and both generation and zero-shot tasks. In particular, for Mamba2-2.7B with W8A8H4 (8-bit weights and activations, 4-bit state caches) quantization, Q-Mamba achieves a 50% reduction in memory consumption with only a 2.13% average accuracy degradation on zero-shot tasks.

1 Introduction

Large language models (LLMs), such as LLaMa (Touvron et al., 2023) and GPT-4 (OpenAI, 2023), have shown exceptional capabilities in general-purpose language understanding (Kaplan et al., 2020; Hoffmann et al., 2022; Tu et al., 2024). However, LLMs based on Transformer architectures still face a significant limitation: the computational cost of their attention mechanism scales quadratically with the sequence length (Vaswani et al., 2017). Therefore, prior works have focused on more efficient attention variants, such as structured state space models (SSMs) (Gu and Dao, 2023; Dao and Gu, 2024; Smith et al., 2023) and linear attention (Peng et al., 2023; Han et al., 2023; Child et al., 2019). Among these, the Mamba architecture (Gu and Dao, 2023; Dao and Gu, 2024) has been shown to match or exceed the downstream accuracy of Transformers on standard language modeling tasks (Waleffe et al., 2024). Following its success in natural language understanding, it has also garnered significant attention in other research areas, such as vision and multimodal tasks (Qiao et al., 2024; Zhu et al., 2024; Peng et al., 2024).

Like Transformers, Mamba language models also operate in two computation phases (Patel et al., 2024). The first is the prefill phase, where all input prompt tokens are processed in parallel through the model's forward pass to generate the first output token. During this phase, Mamba models (Gu and Dao, 2023; Dao and Gu, 2024) employ a hardware-efficient parallel algorithm to compute SSMs (Section 3). The second is the token generation phase, where subsequent output tokens are generated sequentially, relying on the cached state from previous tokens in the sequence. Due to the lack of computational parallelism, this phase tends to be more memory-bound and contributes significantly to the total generation latency.

Although Mamba has successfully replaced the $O(T^2)$ attention module with $O(T)$ selective state space models, our profiling results in Section 4 indicate that it still suffers from two inefficiencies during the generation stage. Firstly, similar to Transformers, the Mamba architecture consists of large linear layers, which require substantial GPU memory and slow down token generation (Figure 2b). Secondly, as larger states allow more information to be stored, states in Mamba are expanded to be N times larger than vanilla activations, where N is the state dimension (128 in Mamba-2 models). Consequently, these state caches account for a significant portion of memory consumption, especially after quantizing weights to low bits (79.6% in Mamba2-2.7B with a batch size of 128, as shown

* The first two authors contributed equally to this work.
† Corresponding author.

Findings of the Association for Computational Linguistics: ACL 2025, pages 10594–10610
July 27 - August 1, 2025

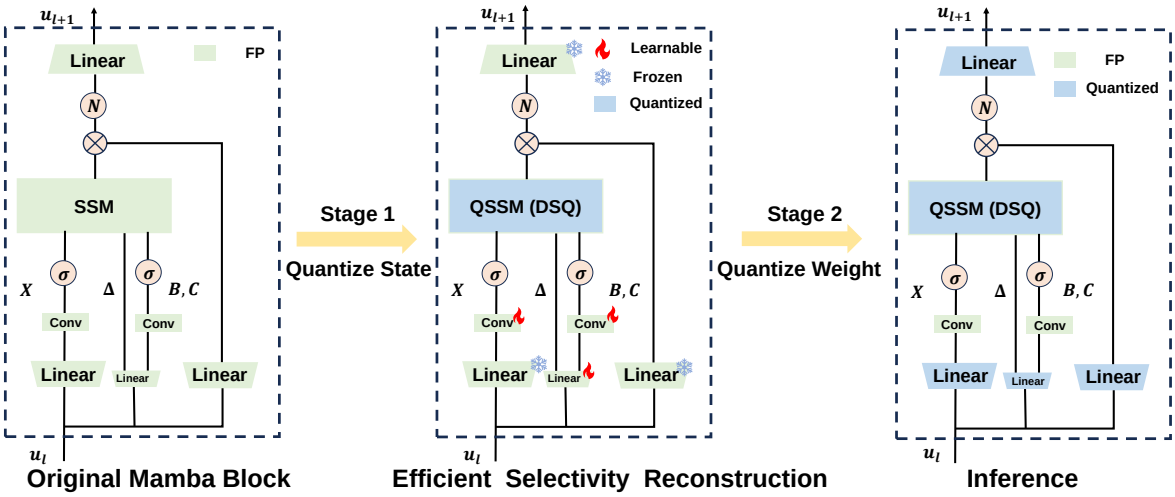

Figure 1: Schematic of the PTQ framework for Mamba. **Left**: The selective parameters B, Δ, and C, along with the SSM inputs x, are generated by the input projections in the Mamba block. **Middle**: After quantizing states using DSQ, ESR updates a small number of selective parameters (approximately 2% of the total) in a block-wise reconstruction manner. **Right**: Finally, we quantize the linear projection into W8A8.

in Figure 2a). In this paper, we address a key question: *Can Mamba models be further optimized through model compression techniques?*

In this paper, we propose **Q-Mamba**, which quantizes both **linear projections** and **state caches** into low-bit integers for Mamba models. Although previous research has successfully quantized Key and Value (KV) caches into low-bit representations in transformers (Liu et al., 2023, 2024b; Hooper et al., 2024), *this work is the first to explore the quantization of state cache in Mamba architectures*. We observe that states exhibit both outlier channels and outlier states (i.e., the state dimension contains large values across all channel dimensions), as shown in Figure 3. Further theoretical analysis reveals this phenomenon results from the computation of the outer products of two activations, each contains outliers in distinct dimensions. This observation motivates us to propose **Decoupled Scale Quantization (DSQ)**, which utilizes separate quantization scales for both dimensions. Additionally, the non-linear nature of the quantization function disrupts the original equivalence between recurrence and quadratic dual form, the latter being essential for efficient training. To address this, we propose Efficient Selectivity Reconstruction (ESR), which simulates quantization errors by quantizing only the final timestep during training. Specifically, ESR updates a small number of selective parameters (approximately 2% of the total) using just 128 training samples in a block-wise reconstruction manner.

Extensive experiments demonstrate that our methods achieve significant performance improvements for Mamba families on various evaluation metrics. To the best of our knowledge, we are the first to achieve W8A8H4 (8-bit linear projection and 4-bit states) for the Mamba architectures. For generation tasks, Q-Mamba achieved perplexities of 12.99 and 16.90 with 4-bit states on WikiText2 (Merity et al., 2017) and C4 (Pal et al., 2023), respectively, while baseline methods degraded to 21.18 and 29.86 even with 6-bit quantization. Additionally, Q-Mamba achieves W8A8H4 quantization for zero-shot tasks with only 2.13% and 2.11% average accuracy degradation on Mamba2-2.7B and Mamba2-1.3B, respectively.

2 Related Works

2.1 Model Quantization

In the current era of burgeoning LLM development, model quantization has also become widely employed (Xiao et al., 2023a; Lin et al., 2023; Frantar et al., 2022; Huang et al., 2024; Xiao et al., 2023b; Chen et al., 2024a). Considering the substantial computational costs of retraining the entire model, much research has focused on Post-Training Quantization (PTQ), which requires only a small amount of calibration data to adjust a limited portion of the parameters. Typically, PTQ methods operate by quantizing and finetuning individual layers or small blocks of consecutive layers (Nagel et al., 2020; Li et al., 2021; Chen et al., 2023). For example, AdaRound (Nagel et al., 2020) uses gradient optimization to determine optimal rounding in a single convolution layer. For LLMs, previous quantization methods have identified significantly larger outliers in activations compared to smaller convolutional neural networks (CNNs). To quantize both weights and activations into INT8, SmoothQuant (Xiao et al., 2023a) mitigates activa-

tion outliers by shifting the quantization difficulty from activations to weights through a mathematically equivalent transformation. These outliers in activations also pose challenges even in scenarios where activations are not quantized (i.e., weight-only quantization) because they amplify the quantization errors of weights when multiplied with activations.

For Mamba models, states have an additional state dimension compared to standard activations, resulting in not only more significant memory consumption but also a distinctive distribution of outliers. To address this issue, we propose two novel methods that enable the quantization of states into 4-bit integers for the first time.

3 Foundations

State Space Model. State space models (SSMs) are a recent class of sequence models for deep learning inspired by a particular continuous system in Equation (2). It maps a **1-dimensional** input sequence $x_t \in \mathbb{R}$ to an output sequence $y_t \in \mathbb{R}$ through a latent state $h_t \in \mathbb{R}^{(N,1)}$:

$$h_t = \bar{A}h_{t-1} + \bar{B}x_t \tag{1a}$$
$$y_t = Ch_t \tag{1b}$$

$$h'(t) = Ah(t) + Bx(t) \tag{2a}$$
$$y(t) = Ch(t) \tag{2b}$$

where $\bar{A} \in \mathbb{R}^{(N,N)}$, $B, \bar{B}, h_{t-1}, h_t, h(t) \in \mathbb{R}^{(N,1)}$, and $C \in \mathbb{R}^{(1,N)}$. Equation (1) can be viewed as discrete versions of a classical continuous system described by Equation (2). Specifically, a timescale parameter Δ is introduced to discretize the parameters A and B into their discrete counterparts, $\bar{A}$ and $\bar{B}$, as explained in the following sections.

Mamba-1. To operate on an input sequence x_t **with** D **channels**, rather than the scalar sequence described earlier, Mamba-1 (Gu and Dao, 2023) assumes that $\bar{A}$ has a diagonal structure and applies the SSM independently to each channel:

$$h_t = \bar{A} \odot h_{t-1} + \bar{B} \odot x_t, \tag{3a}$$
$$y_t = Ch_t, \tag{3b}$$
$$\text{where} \quad \bar{A}, \bar{B}, h_t, h_{t-1} \in \mathbb{R}^{(N,D)}, \quad x_t \in \mathbb{R}^{(1,D)}$$
$$C \in \mathbb{R}^{(1,N)}, \quad y_t \in \mathbb{R}^{(1,D)}$$

where $\odot$ denotes the element-wise product, with automatic broadcasting applied to dimensions of size one.. The discretized parameters are defined as $\bar{A} = \exp(A \odot \Delta)$ and $\bar{B} = B \odot \Delta$, where $A \in \mathbb{R}^{(N,D)}$, $B \in \mathbb{R}^{(N,1)}$, and $\Delta \in \mathbb{R}^{(1,D)}$. Unlike previous non-selective SSMs, Mamba set Δ, B, and C as functions of the inputs rather than fixed parameters. As a result, the variables $\bar{A}$, $\bar{B}$, and C can vary across time steps to dynamically select relevant information from the context.

Mamba-2. To integrate the multi-head design of modern attention mechanisms into Mamba architectures, Mamba-2 (Dao and Gu, 2024) further assumes that $\bar{A}$ and $\bar{B}$ are identical across all dimensions **within the same head** where the head dimension $P \in \{64, 128\}$:

$$h_t = \bar{A} \cdot h_{t-1} + \bar{B} \otimes x_t, \tag{4a}$$
$$y_t = Ch_t, \tag{4b}$$
$$\text{where} \quad h_t, h_{t-1} \in \mathbb{R}^{(N,P)}, \bar{A} \in \mathbb{R}, \bar{B} \in \mathbb{R}^{(N,1)}$$
$$C \in \mathbb{R}^{(1,N)}, \quad x_t, y_t \in \mathbb{R}^{(1,P)}$$

The discretized parameters are still defined as $\bar{A} = \exp(A \odot \Delta)$ and $\bar{B} = B \odot \Delta$. However, unlike Mamba-1, A and Δ are simplified into two scalars within a single head, transforming the operation between $\bar{B}$ and x into an outer product. This simplification improves training efficiency and allows for a larger state size. Consequently, Mamba-2 increases the state size N from 16 in Mamba-1 to 128. Figure 1 left shows the architecture of the Mamba-2 block. The selective parameters B, Δ, and C, along with the SSM inputs x_t, are produced by the input projections in the Mamba block. Specifically, Mamba-2 employs $B = (uW_B)^\top, C = uW_C, \Delta = uW_\Delta, x_t = uW_x$, where $W_B, W_C \in \mathbb{R}^{(D,N)}, W_x \in \mathbb{R}^{(D,P)}, W_\Delta \in \mathbb{R}^{(D,1)}$ and $u \in \mathbb{R}^{(1,D)}$ represents the inputs of Mamba block.

Parallel Training. The recurrent mode described in Equation (1) is used only during the token generation phase, where output tokens are generated sequentially, relying on the cached state from the previous timestep. For parallel training, Mamba (Dao and Gu, 2024) establishes the **equivalence** between selective SSMs and semiseparable matrices, enabling the use of efficient algorithms for structured matrix multiplication (e.g, prefix sum algorithm (Goldberg and Zwick, 1995)). Specifically, Equation (5) represents the **quadratic form** of Equation (1) to compute all timesteps simultaneously:

$$y_t = \sum_{s=0}^{t} C_t \bar{A}^{\times}_{t:s} B_s x_s, \tag{5a}$$
$$y = Mx, M_{ji} := C_j A_j \cdots A_{i+1} B_i, \tag{5b}$$
$$\text{where} \quad \bar{B}, \bar{C}^\top \in \mathbb{R}^{(N,1)}, \quad \bar{A} \in \mathbb{R}^{(N,N)},$$
$$x_t, y_t \in \mathbb{R}, \quad M \in \mathbb{R}^{(T,T)}$$

where M is N-semiseparable matrix. This paper primarily focuses on quantizing the Mamba-2 architecture, which has demonstrated superior performance compared to Mamba-1 across various tasks (Waleffe et al., 2024; Dao and Gu, 2024).

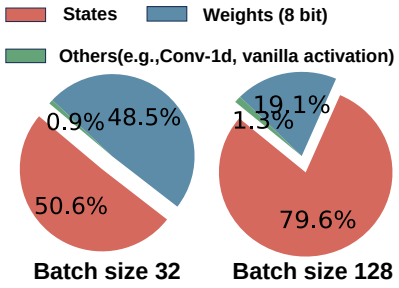

(a)

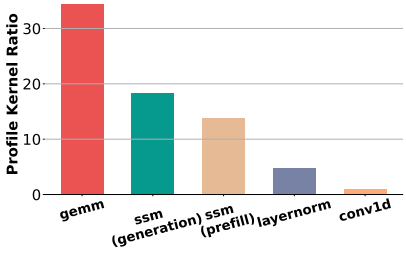

(b)

Figure 2: **Left**: Memory consumption of weights and state caches in Mamba2-2.7B with different batch sizes. **Right**: The Runtime of the Mamba2-2.7B model using NVIDIA profiling tools, with both prompt and generation lengths set to 100 and a batch size of 32.

4 Analysis

In this section, we first analyze the memory consumption and runtime of primary components on the Mamba2-2.7B model, i.e., linear projection, 1D convolution, SSM, and LayerNorm. Based on the results presented in Figures 2a and Figures 2b, we can draw the following conclusions:

Linear projections. Similar to Transformers, large linear layers in Mamba not only require substantial GPU memory but also slow down token generation. When applying quantization to these linear layers, experiments in Section A.1 reveal that outliers exist in specific activation channels of Mamba, particularly in output projections. This phenomenon has also been observed in previous studies on Transformer-based LLMs (Xiao et al., 2023a; Wei et al., 2022).

States in SSMs. As larger states allow more information to be stored, states in Mamba are expanded to be N times larger than vanilla activations, where N is the state dimension (128 in Mamba-2 models). Consequently, these state caches account for a significant portion of memory consumption, especially after quantizing weights to low bits (e.g., 79.6% in Mamba2-2.7B with a batch size of 128, as shown in Figure 2a). This phenomenon not only poses challenges for increasing the batch size to enhance throughput but also prevents further enlargement of state dimensions in Mamba models, which would improve their storage capacity for long contexts (Dao and Gu, 2024; Arora et al., 2024).

To address the above problems, in this paper, we aim to quantize both linear projections and state caches into low-bit integers for Mamba models.

5 Method

5.1 Decoupled Scale Quantization

5.1.1 Outliers in States

For Transformers, particularly LLMs, extensive research (Wei et al., 2022; Xiao et al., 2023a; Liu et al., 2024a) has shown that the presence of outliers extends the range of activation values, which in turn increases quantization errors for normal values. In Mamba models, we observe a similar or even more pronounced issue with outliers in the states. As illustrated in the state distribution visualization in Figure 3(a), outliers are present in both state dimensions (red row) and channel dimensions (green column). Consequently, either per-channel quantization (i.e., using a different quantization step for each channel) or per-state quantization (i.e., using a different quantization step for each state) tends to ignore outliers in the other dimension. As shown in Table 3, the model's performance declines significantly when adopting the above quantization granularity, which calls for a more effective quantization method to address the problem.

5.1.2 Decoupled Scale Quantization

Motivated by the distribution characteristics shown in Figure 3, we present the following theorem, which reveals the underlying causes of this distribution and provides insights for a solution.

Theorem 1. *Assuming $u_t \sim \mathcal{N}(\mathbf{0}, \sigma \boldsymbol{I}_n)$ and A_t is a constant, $B_t = (uW_B)^\top$, $x_t = uW_x$, the variance of states $h_t = A_t \cdot h_{t-1} + B_t \otimes x_t$ can be factorized into two vectors:*

$$Var[h_t] \propto \alpha \cdot \beta^T, \quad \alpha_i = ||W^x_{i,:}||_2^2, \quad \beta_i = ||W^B_{i,:}||_2^2,$$
$$\text{where} \quad \alpha \in \mathbb{R}^P, \quad \beta \in \mathbb{R}^N.$$

The above theorem demonstrates that outliers in the channel dimension P and state dimension N can be attributed to variables x_t and B_t, respectively. A visualization of this phenomenon is provided in Figure 3(b). This motivates us to propose a novel quantization scheme called **Decoupled Scale Quantization (DSQ)**, which utilizes separate quantization scales for the state dimension and the channel dimension:

$$Q(h) = \lfloor \frac{h}{S_{channel} \cdot S_{state}^\top} \rceil \odot (S_{channel} \cdot S_{state}^\top) \quad (6)$$

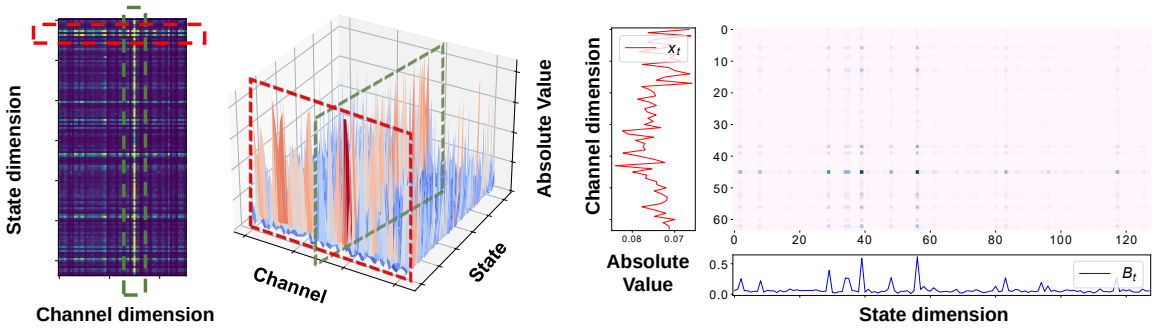

(a) (b)

Figure 3: State distribution in Mamba2-370M. **Left**: Outliers exist in both specific state dimensions (red) and channel dimensions (green). **Right**: Further analysis reveals outliers in channel dimension and state dimension can be attributed to variables x_t and B_t, respectively.

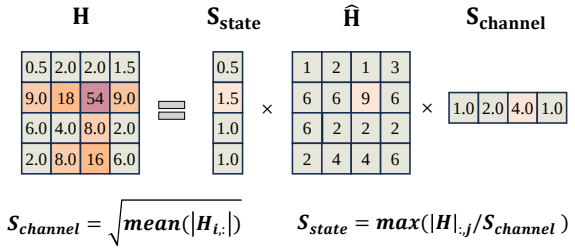

Figure 4: An illustration of DSQ.

where $S_{channel} \in \mathbb{R}^P$, $S_{state} \in \mathbb{R}^N$ and $\lceil \cdot \rfloor$ denotes rounding floating-point values to the nearest integers, while $\odot$ signifies element-wise multiplication.

In this paragraph, we discuss how to compute scales given a specific state. To increase the effective quantization bits, both state and channel scales should accurately represent the magnitude of their respective dimensions. Therefore, an intuitive metric to determine these scales is the vector norm, such as maximum norm ($\|\cdot\|_\infty$) and L^1 norm ($\|\cdot\|_1$). However, in practice, we find that both norms result in even worse performance (see Table 7). Further visualization in Figure 8 shows that these norms are highly sensitive to outliers, resulting in even greater bit wastage. Therefore, for the channel scale, we use the square root of the mean values, which offers a more robust metric that mitigates the influence of outliers. After mitigating most outliers by smoothing the states with channel scale, we employ the MinMax method to compute state scale, which effectively compresses the data range and reduces information loss during quantization:

$$S_{channel,i} = \text{sqrt}(\text{mean}(\text{abs}(h_{i,:}))) = \sqrt{\||h_{i,:}|\|_1} \quad (7)$$

$$S_{state,j} = \max(\text{abs}(\frac{h_{:,j}}{S_{channel}})) = \left\| \frac{|h_{:,j}|}{S_{\text{channel}}} \right\|_\infty \quad (8)$$

where i and j denote subscripts indexing into the channel and state dimensions, respectively. Table 3 demonstrates that DSQ achieves negligible overhead while significantly improving performance.

5.2 Efficient Selectivity Reconstruction

To mitigate the performance loss caused by quantization, PTQ methods often apply block-wise reconstruction (Nagel et al., 2020; Li et al., 2021) with a few data. However, these methods cannot be directly applied to Mamba models due to the challenges introduced in Section 5.2.1.

5.2.1 Challenge in Parallel Training

To minimize memory bandwidth utilization, we store state caches as low-bit elements, then load and dequantize them before computation at the next timestep. This process defines a new sequence transformation through the quantized latent state h_t^q in Equation (9). It is important to distinguish $h_t^q = \bar{A}Q(h_{t-1}^q) + \bar{B}x_t$ from the directly quantized value of the original h_t, denoted as $Q(h_t) = Q(\bar{A}h_{t-1} + \bar{B}x_t)$.

$$h_t^q = \bar{A}Q(h_{t-1}^q) + \bar{B}x_t, \quad (9a)$$
$$y_t^q = Ch_t^q \quad (9b)$$

However, the quantization function leads to non-linear hidden-to-hidden transformation, i.e., h_t^q has a non-linear dependency on h_{t-1}^q. A significant challenge arises because the original parallel training algorithms for linear recurrence are incompatible with the quantization scenario. Specifically, Equation (9) can no longer be reformulated into its quadratic form. A naive approach would involve directly applying Equation (9) for token-by-token

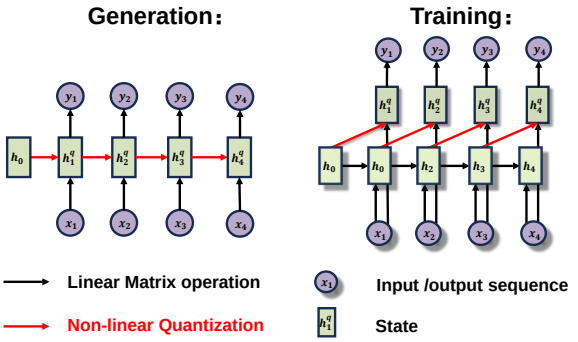

Figure 5: **Left**: In the generation stage, state caches are stored as low-bit elements, then loaded and dequantized before computation at the next timestep. This process introduces a non-linear dependency in the recurrence, which can be parallelized during training **Right**: ESR simulates the quantization errors by quantizing only one step during training, which restores the linear nature of the hidden-to-hidden transformation.

generation. Specially, However, given the large input lengths (e.g., 2048), this method is extremely slow and impractical. Therefore, to apply block-wise reconstruction for Mamba models, it is essential to first investigate how to effectively simulate quantization errors during training

$$\begin{aligned} h_t^q &= \bar{A}_t Q(h_{t-1}^q) + \bar{B}_t x_t \\ &= \bar{A}_t Q(\bar{A}_{t-1} h_{t-2}^q + \bar{B}_{t-1} x_{t-1}) + \bar{B}_t x_t \\ &\neq \bar{A}_t \bar{A}_{t-1} Q(h_{t-2}^q) + \bar{A}_t \bar{B}_{t-1} x_{t-1} + \bar{B}_t x_t \\ &\neq \sum_{s=1}^{t} \bar{A}_s \bar{A}_{s+1} \cdots \bar{A}_t \bar{B}_s x_s \end{aligned} \tag{10}$$

5.2.2 Quantization-Aware State Space Model

Motivated by the linear surrogates proposed in (Martin and Cundy, 2018), we aim to eliminate the non-linear function from the hidden-to-hidden transformation while effectively simulating the quantization errors. To gain insight into this problem, we focus on the difference between the quantized and original states, defined as $\delta_t = h_t^q - h_t$. By substituting δ_t into Equation (9), we observe that δ_t is composed of two parts: the quantization error propagated from the previous timestep, δ_{t-1}, and the quantization error introduced in the current timestep:

$$\begin{aligned} \delta_t = h_t^q - h_t &= \bar{A}_t Q(h_{t-1}^q) + \bar{B}_t x_t - (\bar{A}_t h_{t-1} + \bar{B}_t x_t) \\ &= \bar{A}_t \cdot (Q(h_{t-1}^q) - h_{t-1}) \\ &= \bar{A}_t \cdot (Q(h_{t-1} + \delta_{t-1}) - h_{t-1}) \end{aligned} \tag{11}$$

Assuming that quantization errors δ_{t-1} are sufficiently small compared to the hidden state h_{t-1}, we discard δ_{t-1} and focus only on the quantization errors at the current timestep:

$$\begin{aligned} Q(h_{t-1} + \delta_{t-1}) &\approx Q(h_{t-1}) + Q'(h_{t-1}) \cdot \delta_{t-1} \\ &\approx Q(h_{t-1}) \\ \implies h_t^q &\approx \bar{A}_t Q(h_{t-1}) + \bar{B}_t x_t \end{aligned} \tag{12}$$

Equation (12) enables us to utilize the parallel algorithm to compute h_t at all timesteps, then simulate the quantization errors by quantizing only one step during training, as shown in Figure 5. In the appendix, we present the pseudocode for the parallel training of quantization-aware SSMs for illustrative purposes. Table 4 demonstrates the effectiveness of this quantization simulation, especially in low-bit settings.

5.2.3 Selectivity Guided Adaptation

In the Mamba block, the selective parameters B, Δ, and C, along with the SSM inputs x_t, are generated through input projections, as shown in Figure 1. During block-wise reconstruction, we freeze the linear projections corresponding to the SSM inputs x and z, while keeping the linear projections for selective parameters B, C, and Δ learnable, which is referred to as Selectivity Guided Adaptation (SGA) (Figure 1, middle). Specifically,

$$\min_{\{W_v^q | v \in B,C,\Delta\}} \left\| \mathcal{B}_l(W_v^{FP}, h_t^{FP}; u_l) - \mathcal{B}_l(W_v^q, h_t^q; u_l) \right\|_2, \tag{13}$$

where B_l denotes the mapping function for the l-th Mamba block and u_l represents the block's inputs. W^{FP} and W^q represent the weights of the original model and the quantized model, respectively.

SGA offers two primary advantages: First, the success of Mamba is largely attributed to the selectivity of parameters $\bar{A}$, $\bar{B}$, and $\bar{C}$, which distinguishes it from earlier non-selective SSMs (Gu et al., 2020; Smith et al., 2023). Thus, we hypothesize that this selectivity also plays a critical role in maintaining performance after quantization. Second, SGA reduces the number of learnable parameters, mitigating the risk of overfitting with limited calibration data. For example, in Mamba2-2.7B, learnable parameters account for only about 2% of the total. Note that during this fine-tuning process, the linear layers remain in floating-point values and can be quantized afterward (Figure 1, right).

6 Experiments

6.1 Experiment Setup

Settings. We conduct experiments on the Mamba-2 (Dao and Gu, 2024) models across various model sizes (130M, 370M, 780M, 1.3B, 2.7B). We initialize quantized models using a full-precision model. We utilize the AdamW optimizer with zero weight decay to optimize the learnable parameters in ESR. The learning rate for learnable parameters is set to 1e-3. RedPajama is an

Table 1: Evaluation results of the Mamba-2 models on generation tasks. #W, #A, and #H indicate weight bits, activation bits, and state bits, respectively.

Bits	Method	WikiText2 ↓					C4 ↓				
		130M	370M	780M	1.3B	2.7B	130M	350M	780M	1.3B	2.7B
FP16	-	20.04	14.16	11.81	10.42	9.06	22.25	16.95	14.66	13.27	11.95
W16A16H4	Baseline	976.56	913.34	865.78	1556.15	116.23	542.048	599.49	911.31	529.55	96.93
	Q-Mamba	**45.73**	**22.24**	**19.07**	**15.20**	**11.55**	**39.46**	**26.36**	**22.45**	**19.14**	**14.90**
W16A16H6	Baseline	249.09	134.91	38.04	23.62	13.60	322.97	101.75	38.24	23.73	19.61
	Q-Mamba	**23.79**	**15.33**	**12.69**	**11.37**	**9.59**	**25.11**	**18.27**	**15.66**	**14.52**	**12.57**
W16A16H8	Baseline	20.97	14.83	12.04	10.52	9.11	22.97	17.45	14.85	13.40	**12.01**
	Q-Mamba	**20.49**	**14.26**	**11.86**	**10.51**	**9.11**	**22.64**	**17.05**	**14.73**	**13.39**	12.04
W8A8H4	Baseline	2024.49	1013.15	7225.39	6375.57	364.84	635.86	795.28	10716.17	2788.23	298.57
	Q-Mamba	**53.12**	**27.53**	**23.53**	**17.60**	**12.99**	**46.90**	**32.91**	**26.79**	**21.56**	**16.90**
W8A8H6	Baseline	357.69	220.09	96.51	47.28	21.18	526.59	171.90	79.70	40.46	29.86
	Q-Mamba	**26.75**	**17.27**	**14.51**	**13.05**	**10.84**	**28.18**	**20.53**	**17.79**	**16.45**	**14.46**
W8A8H8	Baseline	23.60	16.69	14.32	**11.85**	10.42	25.51	19.50	17.44	**14.86**	13.73
	Q-Mamba	**22.88**	**15.83**	**13.57**	11.93	**10.36**	**25.01**	**18.84**	**16.80**	15.03	**13.69**

Table 2: Evaluation results of the Mamba-2 models with W8A8H4 (8-bit weights, activations, and 4-bit states) on zero-shot tasks.

Model	Method	OBQA	PIQA	ARC-E	ARC-C	HellaSwag	WINO	AVG ↑
Mamba2-130M	FP	30.6	64.9	47.4	24.2	35.3	52.1	42.41
	Baseline	**30.8**	**63.4**	45.6	**24.6**	**34.1**	51.93	**41.73**
	Q-Mamba	30.0	63.0	**45.7**	23.4	33.9	**53.3**	41.55
Mamba2-370M	FP	32.4	70.5	54.9	26.9	46.9	55.7	47.83
	Baseline	28.6	58.6	46.5	24.9	30.4	53.0	40.34
	Q-Mamba	**32.8**	**68.4**	**53.8**	**26.7**	**43.8**	**54.8**	**46.71**
Mamba2-780M	FP	36.2	72.0	61.0	28.5	54.9	60.2	52.13
	Baseline	32.0	61.8	50.5	25.9	29.5	**57.5**	42.85
	Q-Mamba	**34.2**	**69.6**	**57.3**	**27.6**	**52.1**	55.6	**49.4**
Mamba2-1.3B	FP	37.8	73.2	64.3	33.3	59.9	60.9	54.9
	Baseline	**35.6**	67.1	57.6	29.2	36.8	58.5	47.46
	Q-Mamba	34.8	**72.6**	**62.5**	**31.4**	**55.7**	**59.5**	**52.77**
Mamba2-2.7B	FP	38.8	76.4	69.6	36.4	66.6	64.0	58.63
	Baseline	39.8	73.2	66.8	**36.0**	56.4	59.6	55.30
	Q-Mamba	**40.0**	**73.9**	**66.8**	35.4	**62.0**	**61.0**	**56.52**

open-source reproduction of the pre-training data for LLaMA(Touvron et al., 2023). We employ a calibration dataset consisting of 128 randomly selected 2048-token segments from the RedPajama (Computer, 2023) dataset, except for Mamba2-2.7B, which utilizes 256 samples. The entire training process is facilitated on a single NVIDIA A800 GPU, using a batch size of 1 over 3 epochs. For linear projections, we apply SmoothQuant (Xiao et al., 2023a) with per-token quantization. For state quantization, we use INT8, INT6, and INT4 schemes (e.g., W8A8H4 refers to 8-bit linear projection and 4-bit quantization of the states). We utilize MinMax per-channel quantization (introduced in Section 5.1.2) as state quantization **baseline**.

Evaluation Tasks. We evaluate our methods on both language generation and zero-shot tasks. We report the perplexity on WikiText2 (Merity et al., 2017) and C4 (Pal et al., 2023). For zero-shot tasks, we provide accuracy on datasets including PIQA (Bisk et al., 2020), ARC (Clark et al., 2018), BoolQ (Clark et al., 2019), OpenBookQA (Mihaylov et al., 2018), HellaSwag (Zellers et al., 2019) and Winogrande (Sakaguchi et al., 2020).

6.2 Main Results

Generation Tasks.

We evaluate generation tasks in recurrent mode with a sequence length of 2048. The results in Table 1 demonstrate the effectiveness of Q-Mamba across various quantization configurations. For INT8 state quantization, we exclusively utilize DSQ without ESR, as DSQ alone achieves nearly lossless quantization compared to full-precision models. Without our methods, states are limited to 8-bit quantization, with lower-bit quantization, such as 6-bit, leading to significant performance degradation, e.g., 23.62 perplexity for Mamba2-1.3B on the WikiText2 dataset. In contrast, Q-

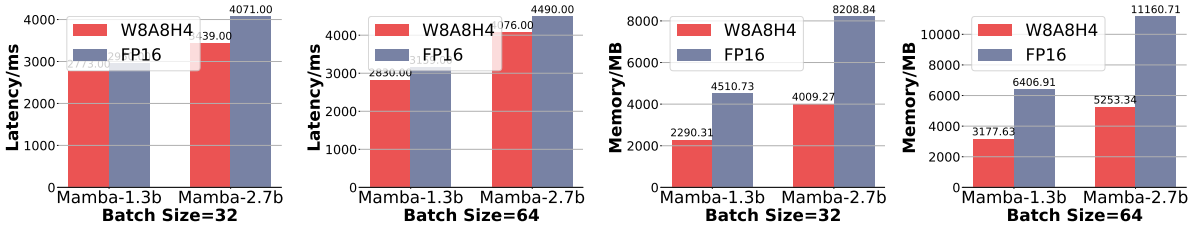

Figure 6: Inference latency and memory usage of the Mamba2 models with different batch sizes on NVIDIA GeForce RTX 3090.

Table 3: The performance and overheads of different quantization methods on Mamba2-370M. P and N denote channel and state dimensions, respectively.

Granularity	WikiText2 ↓	Overheads
Per-tensor	4815.83	$\frac{1}{P\times N}$
Per-channel	3364.58	$\frac{1}{P}$
Per-state	947.88	$\frac{1}{N}$
DSQ	**25.73**	$\frac{1}{P}+\frac{1}{N}$

Table 4: Efficacy of each component in ESR. ESR enables adjusting parameters of Mamba blocks after quantizing states **in block-wise reconstruction**. When combined with SGA, these two techniques further enhance performance.

Method	WikiText2 ↓	C4 ↓
DSQ w/o ESR	25.73	29.94
DSQ+ESR (w/o SGA)	23.73	28.19
DSQ+ESR (w/ SGA)	**21.92**	**25.99**

Mamba facilitates nearly lossless 6-bit quantization, achieving a minimal degradation of only 0.53 perplexity for Mamba2-2.7B and 0.88 perplexity for Mamba2-1.3B. Moreover, Q-Mamba enables effective 4-bit quantization and is compatible with the linear projection quantization approach. For example, Q-Mamba achieves 12.99 perplexity in W8A8H4 quantization settings for the Mamba2-2.7B model.

Zero-shot Tasks. We evaluate the performance of Q-Mamba on zero-shot tasks using the lm-eval-harness (Gao et al., 2024) framework in Table 2. Q-Mamba significantly improves the average accuracy across various models. For example, it increases the average accuracy by 6.37%, 6.55%, and 5.31% on the 370M, 780M, and 1.3B models. Additionally, for Mamba2-2.7B and Mamba2-1.3B, Q-Mamba achieves W8A8H4 quantization with only 2.13% and 2.11% accuracy degradation.

6.3 Ablations

In this section, we conduct experiments to validate the efficacy of each component, as well as the design choices for DSQ. Due to page limitations, we include additional ablations in Section A.4 of the Appendix.

Effectiveness of each component. Table 3 demonstrates that DSQ is essential in state quantization. The model's performance declines significantly when per-channel or per-state quantization methods are adopted. By decoupling scales in the state and channel dimensions, DSQ mitigates outliers in both dimensions with negligible overhead. Table 4 shows that we can further enhance model performance in block-wise reconstruction with ESR. Furthermore, finetuning selective parameters instead of all parameters can help avoid overfitting and yield better results.

6.4 Efficiency

Figure 6 presents the memory and time requirements for inference using Mamba2 models. For W8A8 linear projections, we employ CUDA INT8 GEMM, following the approach of SmoothQuant (Xiao et al., 2023a). For INT4 state quantization, we implement SSM kernels with quantized and packed states with Triton (Tillet et al., 2019), a language and compiler for CUDA computation. Both the input context and generation length are set to 100. The results show that the quantized models can reduce memory usage by half while maintaining or even improving inference latency.

7 Conclusion

In this paper, we propose Q-Mamba, a novel quantization framework designed for state caches in Mamba models. We conduct a theoretical analysis of outliers in states and propose Decoupled Scale Quantization (DSQ) which decouple scales in the state and channel dimensions, DSQ mitigates outliers in both dimensions while introducing negligible overhead. To further boost performance through block-wise reconstruction, we propose Efficient Selectivity Reconstruction (ESR), which includes a novel quantization simulation method that enables efficient fine-tuning of selective parameters with parallel scan mode. In conclusion, Q-Mamba demonstrates that Mamba architectures have the

potential for further optimization when combined with other model compression techniques.

Limitations

In this paper, we propose Q-Mamba, a novel quantization framework designed for state caches in Mamba models. Although Q-Mamba reduces memory usage by half and achieves a 1.18x speedup on GPUs with only a 2.13% average accuracy degradation on zero-shot tasks, maximizing acceleration in large language models LLMs based on Mamba via quantization requires greater hardware support. Previous research on hardware accelerators has primarily focused on LLMs (Wang et al., 2021; Sridharan et al., 2023) based on transformer architectures. We hope this paper will inspire more researchers to focus on developing customized hardware for low-bit SSM models.

Acknowledgments

This work was supported in part by the National Key R&D Program of China (2022ZD0116406), the Science and Technology Major Special Program of Jiangsu (Grants No.BG2024028), the Natural Science Foundation of Jiangsu Province (No.BK20243051), and the Jiangsu Key Research and Development Plan (No.BE2023016).

References

Simran Arora, Sabri Eyuboglu, Michael Zhang, Aman Timalsina, Silas Alberti, Dylan Zinsley, James Zou, Atri Rudra, and Christopher Ré. 2024. Simple linear attention language models balance the recall-throughput tradeoff. *CoRR*, abs/2402.18668.

Yonatan Bisk, Rowan Zellers, Ronan Le Bras, Jianfeng Gao, and Yejin Choi. 2020. PIQA: reasoning about physical commonsense in natural language. In *The Thirty-Fourth AAAI Conference on Artificial Intelligence, AAAI 2020, The Thirty-Second Innovative Applications of Artificial Intelligence Conference, IAAI 2020, The Tenth AAAI Symposium on Educational Advances in Artificial Intelligence, EAAI 2020, New York, NY, USA, February 7-12, 2020*, pages 7432–7439. AAAI Press.

Tianqi Chen, Zhe Li, Weixiang Xu, Zeyu Zhu, Dong Li, Lu Tian, Emad Barsoum, Peisong Wang, and Jian Cheng. 2024a. Ternaryllm: Ternarized large language model. *arXiv preprint arXiv:2406.07177*.

Tianqi Chen, Weixiang Xu, Weihan Chen, Peisong Wang, and Jian Cheng. 2023. Towards efficient and accurate winograd convolution via full quantization. In *Proceedings of the 37th International Conference on Neural Information Processing Systems*, NIPS '23, Red Hook, NY, USA. Curran Associates Inc.

Yingfa Chen, Xinrong Zhang, Shengding Hu, Xu Han, Zhiyuan Liu, and Maosong Sun. 2024b. Stuffed mamba: State collapse and state capacity of rnn-based long-context modeling. *Preprint*, arXiv:2410.07145.

Rewon Child, Scott Gray, Alec Radford, and Ilya Sutskever. 2019. Generating long sequences with sparse transformers. *URL https://openai.com/blog/sparse-transformers*.

Christopher Clark, Kenton Lee, Ming-Wei Chang, Tom Kwiatkowski, Michael Collins, and Kristina Toutanova. 2019. Boolq: Exploring the surprising difficulty of natural yes/no questions. In *Proceedings of the 2019 Conference of the North American Chapter of the Association for Computational Linguistics: Human Language Technologies, NAACL-HLT 2019, Minneapolis, MN, USA, June 2-7, 2019, Volume 1 (Long and Short Papers)*, pages 2924–2936. Association for Computational Linguistics.

Peter Clark, Isaac Cowhey, Oren Etzioni, Tushar Khot, Ashish Sabharwal, Carissa Schoenick, and Oyvind Tafjord. 2018. Think you have solved question answering? try arc, the AI2 reasoning challenge. *CoRR*, abs/1803.05457.

Together Computer. 2023. Redpajama: an open dataset for training large language models.

Tri Dao and Albert Gu. 2024. Transformers are ssms: Generalized models and efficient algorithms through structured state space duality. *Preprint*, arXiv:2405.21060.

Elias Frantar, Saleh Ashkboos, Torsten Hoefler, and Dan Alistarh. 2022. GPTQ: accurate post-training quantization for generative pre-trained transformers. *CoRR*, abs/2210.17323.

Leo Gao, Jonathan Tow, Baber Abbasi, Stella Biderman, Sid Black, Anthony DiPofi, Charles Foster, Laurence Golding, Jeffrey Hsu, Alain Le Noac'h, Haonan Li, Kyle McDonell, Niklas Muennighoff, Chris Ociepa, Jason Phang, Laria Reynolds, Hailey Schoelkopf, Aviya Skowron, Lintang Sutawika, Eric Tang, Anish Thite, Ben Wang, Kevin Wang, and Andy Zou. 2024. A framework for few-shot language model evaluation.

Tal Goldberg and Uri Zwick. 1995. Optimal deterministic approximate parallel prefix sums and their applications. In *Third Israel Symposium on Theory of Computing and Systems, ISTCS 1995, Tel Aviv, Israel, January 4-6, 1995, Proceedings*, pages 220–228. IEEE Computer Society.

Albert Gu and Tri Dao. 2023. Mamba: Linear-time sequence modeling with selective state spaces. *CoRR*, abs/2312.00752.

Albert Gu, Tri Dao, Stefano Ermon, Atri Rudra, and Christopher Ré. 2020. Hippo: Recurrent memory with optimal polynomial projections.

In *Advances in Neural Information Processing Systems 33: Annual Conference on Neural Information Processing Systems 2020, NeurIPS 2020, December 6-12, 2020, virtual*.

Albert Gu, Karan Goel, and Christopher Ré. 2022. Efficiently modeling long sequences with structured state spaces. In *The Tenth International Conference on Learning Representations, ICLR 2022, Virtual Event, April 25-29, 2022*. OpenReview.net.

Dongchen Han, Tianzhu Ye, Yizeng Han, Zhuofan Xia, Shiji Song, and Gao Huang. 2023. Agent attention: On the integration of softmax and linear attention. *CoRR*, abs/2312.08874.

Jordan Hoffmann, Sebastian Borgeaud, Arthur Mensch, Elena Buchatskaya, Trevor Cai, Eliza Rutherford, Diego de Las Casas, Lisa Anne Hendricks, Johannes Welbl, Aidan Clark, Tom Hennigan, Eric Noland, Katie Millican, George van den Driessche, Bogdan Damoc, Aurelia Guy, Simon Osindero, Karen Simonyan, Erich Elsen, Jack W. Rae, Oriol Vinyals, and Laurent Sifre. 2022. Training compute-optimal large language models. *CoRR*, abs/2203.15556.

Coleman Hooper, Sehoon Kim, Hiva Mohammadzadeh, Michael W. Mahoney, Yakun Sophia Shao, Kurt Keutzer, and Amir Gholami. 2024. Kvquant: Towards 10 million context length LLM inference with KV cache quantization. *CoRR*, abs/2401.18079.

Wei Huang, Xudong Ma, Haotong Qin, Xingyu Zheng, Chengtao Lv, Hong Chen, Jie Luo, Xiaojuan Qi, Xianglong Liu, and Michele Magno. 2024. How good are low-bit quantized llama3 models? an empirical study. *Preprint*, arXiv:2404.14047.

Jared Kaplan, Sam McCandlish, Tom Henighan, Tom B. Brown, Benjamin Chess, Rewon Child, Scott Gray, Alec Radford, Jeffrey Wu, and Dario Amodei. 2020. Scaling laws for neural language models. *CoRR*, abs/2001.08361.

Yuhang Li, Ruihao Gong, Xu Tan, Yang Yang, Peng Hu, Qi Zhang, Fengwei Yu, Wei Wang, and Shi Gu. 2021. BRECQ: pushing the limit of post-training quantization by block reconstruction. In *9th International Conference on Learning Representations, ICLR 2021, Virtual Event, Austria, May 3-7, 2021*. OpenReview.net.

Ji Lin, Jiaming Tang, Haotian Tang, Shang Yang, Xingyu Dang, and Song Han. 2023. AWQ: activation-aware weight quantization for LLM compression and acceleration. *CoRR*, abs/2306.00978.

Zechun Liu, Barlas Oguz, Changsheng Zhao, Ernie Chang, Pierre Stock, Yashar Mehdad, Yangyang Shi, Raghuraman Krishnamoorthi, and Vikas Chandra. 2023. LLM-QAT: data-free quantization aware training for large language models. *CoRR*, abs/2305.17888.

Zechun Liu, Changsheng Zhao, Igor Fedorov, Bilge Soran, Dhruv Choudhary, Raghuraman Krishnamoorthi, Vikas Chandra, Yuandong Tian, and Tijmen Blankevoort. 2024a. Spinquant: LLM quantization with learned rotations. *CoRR*, abs/2405.16406.

Zirui Liu, Jiayi Yuan, Hongye Jin, Shaochen Zhong, Zhaozhuo Xu, Vladimir Braverman, Beidi Chen, and Xia Hu. 2024b. KIVI: A tuning-free asymmetric 2bit quantization for KV cache. In *Forty-first International Conference on Machine Learning, ICML 2024, Vienna, Austria, July 21-27, 2024*. OpenReview.net.

Eric Martin and Chris Cundy. 2018. Parallelizing linear recurrent neural nets over sequence length. In *6th International Conference on Learning Representations, ICLR 2018, Vancouver, BC, Canada, April 30 - May 3, 2018, Conference Track Proceedings*. OpenReview.net.

Harsh Mehta, Ankit Gupta, Ashok Cutkosky, and Behnam Neyshabur. 2023. Long range language modeling via gated state spaces. In *The Eleventh International Conference on Learning Representations, ICLR 2023, Kigali, Rwanda, May 1-5, 2023*. OpenReview.net.

Stephen Merity, Caiming Xiong, James Bradbury, and Richard Socher. 2017. Pointer sentinel mixture models. In *5th International Conference on Learning Representations, ICLR 2017, Toulon, France, April 24-26, 2017, Conference Track Proceedings*. OpenReview.net.

Todor Mihaylov, Peter Clark, Tushar Khot, and Ashish Sabharwal. 2018. Can a suit of armor conduct electricity? A new dataset for open book question answering. In *Proceedings of the 2018 Conference on Empirical Methods in Natural Language Processing, Brussels, Belgium, October 31 - November 4, 2018*, pages 2381–2391. Association for Computational Linguistics.

Markus Nagel, Rana Ali Amjad, Mart van Baalen, Christos Louizos, and Tijmen Blankevoort. 2020. Up or down? adaptive rounding for post-training quantization. In *Proceedings of the 37th International Conference on Machine Learning, ICML 2020, 13-18 July 2020, Virtual Event*, volume 119 of *Proceedings of Machine Learning Research*, pages 7197–7206. PMLR.

OpenAI. 2023. GPT-4 technical report. *CoRR*, abs/2303.08774.

Kuntal Kumar Pal, Kazuaki Kashihara, Ujjwala Anantheswaran, Kirby C. Kuznia, Siddhesh Jagtap, and Chitta Baral. 2023. Exploring the limits of transfer learning with unified model in the cybersecurity domain. *CoRR*, abs/2302.10346.

Pratyush Patel, Esha Choukse, Chaojie Zhang, Aashaka Shah, Íñigo Goiri, Saeed Maleki, and Ricardo Bianchini. 2024. Splitwise: Efficient generative LLM inference using phase splitting.

In *51st ACM/IEEE Annual International Symposium on Computer Architecture, ISCA 2024, Buenos Aires, Argentina, June 29 - July 3, 2024*, pages 118–132. IEEE.

Bo Peng, Eric Alcaide, Quentin Anthony, Alon Albalak, Samuel Arcadinho, Stella Biderman, Huanqi Cao, Xin Cheng, Michael Chung, Leon Derczynski, Xingjian Du, Matteo Grella, Kranthi Kiran GV, Xuzheng He, Haowen Hou, Przemyslaw Kazienko, Jan Kocon, Jiaming Kong, Bartlomiej Koptyra, Hayden Lau, Jiaju Lin, Krishna Sri Ipsit Mantri, Ferdinand Mom, Atsushi Saito, Guangyu Song, Xiangru Tang, Johan S. Wind, Stanislaw Wozniak, Zhenyuan Zhang, Qinghua Zhou, Jian Zhu, and Rui-Jie Zhu. 2023. RWKV: reinventing rnns for the transformer era. In *Findings of the Association for Computational Linguistics: EMNLP 2023, Singapore, December 6-10, 2023*, pages 14048–14077. Association for Computational Linguistics.

Siran Peng, Xiangyu Zhu, Haoyu Deng, Liang-Jian Deng, and Zhen Lei. 2024. Fusionmamba: Efficient remote sensing image fusion with state space model. *IEEE Trans. Geosci. Remote. Sens.*, 62:1–16.

Yanyuan Qiao, Zheng Yu, Longteng Guo, Sihan Chen, Zijia Zhao, Mingzhen Sun, Qi Wu, and Jing Liu. 2024. Vl-mamba: Exploring state space models for multimodal learning. *CoRR*, abs/2403.13600.

Keisuke Sakaguchi, Ronan Le Bras, Chandra Bhagavatula, and Yejin Choi. 2020. Winogrande: An adversarial winograd schema challenge at scale. In *The Thirty-Fourth AAAI Conference on Artificial Intelligence, AAAI 2020, The Thirty-Second Innovative Applications of Artificial Intelligence Conference, IAAI 2020, The Tenth AAAI Symposium on Educational Advances in Artificial Intelligence, EAAI 2020, New York, NY, USA, February 7-12, 2020*, pages 8732–8740. AAAI Press.

Jimmy T. H. Smith, Andrew Warrington, and Scott W. Linderman. 2023. Simplified state space layers for sequence modeling. In *The Eleventh International Conference on Learning Representations, ICLR 2023, Kigali, Rwanda, May 1-5, 2023*. OpenReview.net.

Shrihari Sridharan, Jacob R. Stevens, Kaushik Roy, and Anand Raghunathan. 2023. X-former: In-memory acceleration of transformers. *IEEE Trans. Very Large Scale Integr. Syst.*, 31(8):1223–1233.

Philippe Tillet, Hsiang-Tsung Kung, and David Cox. 2019. Triton: an intermediate language and compiler for tiled neural network computations. In *Proceedings of the 3rd ACM SIGPLAN International Workshop on Machine Learning and Programming Languages*, pages 10–19.

Hugo Touvron, Thibaut Lavril, Gautier Izacard, Xavier Martinet, Marie-Anne Lachaux, Timothée Lacroix, Baptiste Rozière, Naman Goyal, Eric Hambro, Faisal Azhar, Aurélien Rodriguez, Armand Joulin, Edouard Grave, and Guillaume Lample. 2023. Llama: Open and efficient foundation language models. *CoRR*, abs/2302.13971.

Xiaoguang Tu, Zhi He, Yi Huang, Zhi-Hao Zhang, Ming Yang, and Jian Zhao. 2024. An overview of large ai models and their applications. *Visual Intelligence*, 2.

Ashish Vaswani, Noam Shazeer, Niki Parmar, Jakob Uszkoreit, Llion Jones, Aidan N. Gomez, Lukasz Kaiser, and Illia Polosukhin. 2017. Attention is all you need. In *Advances in Neural Information Processing Systems 30: Annual Conference on Neural Information Processing Systems 2017, December 4-9, 2017, Long Beach, CA, USA*, pages 5998–6008.

Roger Waleffe, Wonmin Byeon, Duncan Riach, Brandon Norick, Vijay Korthikanti, Tri Dao, Albert Gu, Ali Hatamizadeh, Sudhakar Singh, Deepak Narayanan, Garvit Kulshreshtha, Vartika Singh, Jared Casper, Jan Kautz, Mohammad Shoeybi, and Bryan Catanzaro. 2024. An empirical study of mamba-based language models. *CoRR*, abs/2406.07887.

Hanrui Wang, Zhekai Zhang, and Song Han. 2021. Spatten: Efficient sparse attention architecture with cascade token and head pruning. In *IEEE International Symposium on High-Performance Computer Architecture, HPCA 2021, Seoul, South Korea, February 27 - March 3, 2021*, pages 97–110. IEEE.

Junxiong Wang, Jing Nathan Yan, Albert Gu, and Alexander M. Rush. 2023. Pretraining without attention. In *Findings of the Association for Computational Linguistics: EMNLP 2023, Singapore, December 6-10, 2023*, pages 58–69. Association for Computational Linguistics.

Xiuying Wei, Yunchen Zhang, Xiangguo Zhang, Ruihao Gong, Shanghang Zhang, Qi Zhang, Fengwei Yu, and Xianglong Liu. 2022. Outlier suppression: Pushing the limit of low-bit transformer language models. In *NeurIPS*.

Guangxuan Xiao, Ji Lin, Mickaël Seznec, Hao Wu, Julien Demouth, and Song Han. 2023a. Smoothquant: Accurate and efficient post-training quantization for large language models. In *International Conference on Machine Learning, ICML 2023, 23-29 July 2023, Honolulu, Hawaii, USA*, volume 202 of *Proceedings of Machine Learning Research*, pages 38087–38099. PMLR.

Yisong Xiao, Aishan Liu, Tianyuan Zhang, Haotong Qin, Jinyang Guo, and Xianglong Liu. 2023b. Robustmq: benchmarking robustness of quantized models. *Vis. Intell.*, 1(1).

Rowan Zellers, Ari Holtzman, Yonatan Bisk, Ali Farhadi, and Yejin Choi. 2019. Hellaswag: Can a machine really finish your sentence? In *Proceedings of the 57th Conference of the Association for Computational Linguistics, ACL 2019, Florence, Italy, July 28- August 2, 2019, Volume 1: Long Papers*, pages 4791–4800. Association for Computational Linguistics.

Lianghui Zhu, Bencheng Liao, Qian Zhang, Xinlong Wang, Wenyu Liu, and Xinggang Wang. 2024. Vision mamba: Efficient visual representation learning with bidirectional state space model. *CoRR*, abs/2401.09417.

A Appendix

A.1 Previous PTQ methods on Mamba

In Section 4, we analyze the quantization of linear projections in Mamba models. Here, we provide more detailed results about previous PTQ methods on Mamba-1 and Mamba-2 models. We will analyze the difference between Mamba-1 models and Mamba-2 models from a view of model quantization. The results presented in Table 5 indicate that Mamba2 models exhibit greater robustness to quantization compared to Mamba1 models. Further analysis in Figure 7 reveals that this improvement is largely due to the additional LayerNorm applied before the output projection in Mamba2, which helps to reduce outliers to a certain extent. Moreover, this LayerNorm simplifies the implementation of previous PTQ methods based on smoothing between weights and activations, such as SmoothQuant (Xiao et al., 2023a) and AWQ (Lin et al., 2023). As a result, this paper primarily focuses on Mamba2 models, which not only feature larger state dimensions but are also more amenable to quantization.

A.2 Proof

Theorem 2. *Assuming $u_t \sim \mathcal{N}(\mathbf{0}, \sigma \boldsymbol{I}_n)$ and A_t is a constant, $B_t = (uW_B)^\top$, $x_t = uW_x$, the variance of states $h_t = A_t \cdot h_{t-1} + B_t \otimes x_t$ can be factorized into two vectors:*

$$Var[h_t] \propto \alpha \cdot \beta^T, \quad \alpha_i = ||W^x_{i,:}||_2^2, \quad \beta_i = ||W^B_{i,:}||_2^2,$$
$$where \quad \alpha \in \mathbb{R}^P, \quad \beta \in \mathbb{R}^N.$$

Proof. Firstly, we can reformulate Equation (**??**) as a prefix sum:

$$h_t = \sum_i^t A_{i:t} x_i B_i^\top, \quad where \quad A_{i:t} = A_i \times A_{i+1} \times \dots A_t \tag{14}$$

Then, we can compute the mean of states h_t as follows:

$$\begin{aligned}
\mathbb{E}[h_t] &= \sum_i^t A_{i:t} \mathbb{E}[x_i B_i^\top] \\
&= \sum_i^t A_{i:t} \mathbb{E}[W^x u_i u_i^\top {W^b}^\top] \\
&= \sum_i^t A_{i:t} W^x \mathbb{E}[u_i u_i^\top] {W^b}^\top \\
&= \sum_i^t A_{i:t} \sigma W^x {W^b}^\top
\end{aligned} \tag{15}$$

After computing the mean of the states, we can similarly compute the variance of the states h_t.

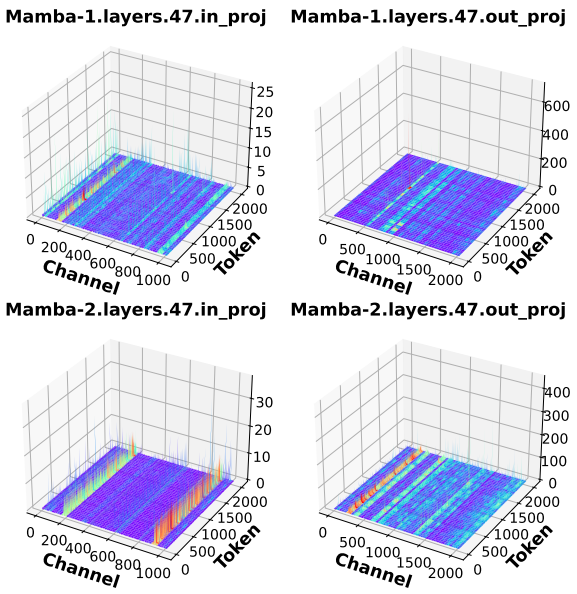

Figure 7: Visualization of inputs for linear projections. The out projection suffers from more severe outliers compared to the in projection.

Model	Method	WikiText2	C4
Mamba1-370M	FP	14.31	17.23
	W8A8	18.95	23.04
	W8A8+SQ	16.17	19.85
	W4A16+ GPTQ	16.03	19.06
Mamba2-370M	FP	14.16	16.95
	W8A8	17.14	20.10
	W8A8+SQ	15.71	18.72
	W4A16+GPTQ	15.81	18.71

Table 5: Different PTQ methods for Mamba models. Mamba-1 models suffer much more serious outliers in output projections because of the absence of LayerNorm before it.

The equality (a) is attributed to Lemma 1. □

$$\begin{aligned}\mathrm{Var}[x_i B_i^\top] &= \mathbb{E}[(W^x u_i u_i^\top {W^b}^\top - \sigma W^x {W^b}^\top)] \\ &= \mathbb{E}[(W^x (u_i u_i^\top) {W^b}^\top)^2] \\ &\quad - 2\sigma \cdot \mathbb{E}[W^x {W^b}^\top \odot (W^x u_i u_i^\top {W^b}^\top)] \\ &\quad + (\sigma W^x {W^b}^\top)^2 \\ &\overset{(a)}{=} \sigma^2 \alpha \cdot \beta^\top + 2\sigma^2 \cdot (W^x W_b^\top)^2 \\ &\quad - 2\sigma^2 \cdot (W^x W_b^\top)^2 + \sigma^2 \cdot (W^x {W^b}^\top)^2 \\ &= \sigma^2 \alpha \cdot \beta^\top + \sigma^2 \cdot (W^x {W^b}^\top)^2 \end{aligned} \tag{16}$$

Here, we assume that the second term $(W^x {W^b}^\top)^2$ is sufficiently small compared to $\alpha \cdot \beta^\top$, and then we obtain:

$$\mathrm{Var}[h_t] = \quad = (\sigma^2 \sum_i^t A_{i:t}) \cdot (\alpha \cdot \beta^\top) \tag{17}$$

Lemma 1. *Assuming $z \sim \mathcal{N}(\mathbf{0}, \boldsymbol{I}_n)$, $w_1, w_2 \in \mathbb{R}^n$, we have the following conclusions:*

$$\mathbb{E}[({w_1}^\top z)^2 ({w_2}^\top z)^2] = ||w_1||_2^2 \cdot ||w_2||_2^2 + 2({w_1}^\top w_2)^2 \tag{18}$$

Proof. Let A and B be two arbitrary symmetric

matrices, we have:

$$\begin{aligned}
\mathbb{E}\left[x^\top Ax \cdot x^\top Bx\right] &= \mathbb{E}\left[\sum_{i,j} x_i a_{ij} x_j \sum_{k,l} x_k b_{kl} x_l\right] \\
&= \mathbb{E}\left[\sum_{i,k} a_{ii} b_{kk} x_i^2 x_k^2 + 4\sum_{i<j} a_{ij} b_{ij} x_i^2 \right. \\
&= \sum_{i,k} a_{ii} b_{kk} + 2\sum_{i} a_{ii} b_{ii} \\
&\quad + 2\left(\sum_{i,j} a_{ij} b_{ij} - \sum_{i} a_{ii} b_{ii}\right) \\
&= \sum_{i} a_{ii} \sum_{k} b_{kk} + 2\sum_{i,j} a_{ij} b_{ij} \\
&= \mathrm{Tr}(A)\mathrm{Tr}(B) + 2\mathrm{Tr}(AB)
\end{aligned} \tag{19}$$

A special case occurs when $A = w_1 {w_1}^\top$ and $B = w_2 {w_2}^\top$:

$$\mathbb{E}[({w_1}^\top z)^2 ({w_2}^\top z)^2] = ||w_1||_2^2 \cdot ||w_2||_2^2 + 2({w_1}^\top w_2)^2 \tag{20}$$

□

Although this theorem imposes strict constraints on the SSM inputs u_t (Gaussian distribution) and A_t (constant), it sufficiently reveals the following fact: outliers in the channel dimension P and state dimension N can be attributed to the variables $x_t \in \mathbb{R}^{(T,P)}$ and $B_t \in \mathbb{R}^{(T,N)}$, respectively. Figure 3 provides a visualization of this phenomenon.

A.3 Related Works about State Space Mode

Transformer-based LLMs (Touvron et al., 2023; OpenAI, 2023) suffer from the computational cost of their attention mechanism scales quadratically with sequence length. Consequently, much research has focused on developing more efficient variants of attention, such as structured state space models (SSMs) (Gu and Dao, 2023; Dao and Gu, 2024; Smith et al., 2023). The original structured SSMs (S4) (Gu et al., 2022) were linear time-invariant (LTI) systems motivated by continuous-time online memorization. Many variants of structured SSMs have been proposed, for example, Gated SSM architectures, such as GSS (Mehta et al., 2023) and BiGS (Wang et al., 2023), incorporate a gating mechanism into SSMs for language modeling. Recently, the Mamba (Gu and Dao, 2023; Dao and Gu, 2024) architecture demonstrates promising performance on standard language modeling tasks (Waleffe et al., 2024), as well as on vision and multimodal tasks (Zhu et al., 2024; Qiao et al., 2024). Mamba showed that state expansion and selective ability are crucial for selecting and memorizing useful information in the hidden states.

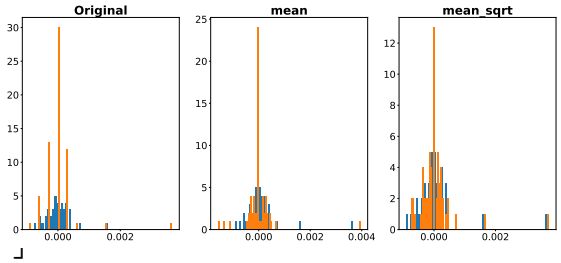

Figure 8: An illustration of how DSQ enhances performance.

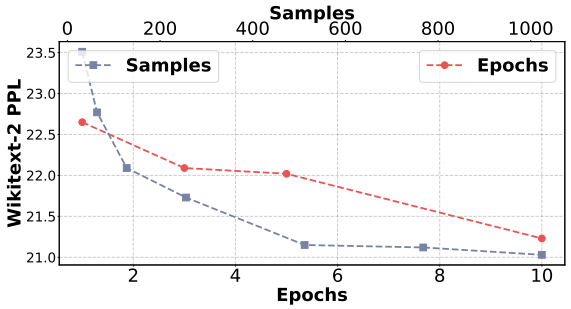

Figure 9: Illustration of WikiText2 perplexity of W16A16H4 quantization with different training samples and epochs.

A.4 More Ablation Studies

In this section, we conduct more experiments to validate the efficacy of design choices for DSQ, training epochs, and calibration data size. We also provide visualizations of DSQ and a detailed analysis of the impact of trainable parameters in ESR.

Visualization of DSQ. Figure 8 illustrates how DSQ improves performance. The presence of outliers causes MinMax quantization to waste a significant portion of available quantization slots, resulting in large rounding errors. Although introducing channel scales $S_{channel}$ helps make the quantization slots non-uniform, the mean norm remains sensitive to outliers, even unexpectedly amplifying them (as shown in the middle figure).

Trainable parameters in ESR. Table 8 demonstrates the effectiveness of our choice of trainable parameters in ESR: Fine-tuning selective parameters (B, C, and Δ), layer normalization, and convolution yields the best perplexity. In contrast, including x and z results in worse performance. We attribute this to the fact that fine-tuning all parameters can lead to overfitting and necessitates end-to-end training.

Calibration Datasets. We conducted ablation studies on Mamba-2-1.3B using three calibration datasets (WikiText2, PTB, RedPajama). The results show minimal performance variation across datasets (Table 6) because we used only 128 examples, and fine-tuning affected only 2% of the parameters.

Table 6: Calibration dataset ablation (W16A16H4 quantization).

Calibration Dataset	WikiText2	C4
WikiText2	**14.03**	18.35
PTB	14.24	**18.12**
RedPajama	14.78	18.48

Samples and epochs for block-wise reconstruction. To ensure training efficiency, we set 3 epochs and 128 samples for all experiments, except for Mamba2-2.7B, where we use 256 samples. However, as shown in Figure 9, performance can be further improved by increasing the number of training samples and epochs.

Table 7: Impact of different design choices for DSQ. Experiments are conducted on Mamba2-370M with W16A16H4 quantization.

Method	WikiText2 ↓	C4 ↓
abs.max	inf	inf
abs.max.sqrt	42.88	46.61
abs.mean	inf	inf
abs.mean.sqrt	**25.73**	**29.94**

Design choices of DSQ. The results in Table 7 highlight the critical importance of selecting appropriate quantization scales for DSQ. Firstly, squaring the norms as quantization scales is essential for maintaining stability. Furthermore, using mean values yields superior performance compared to relying on maximum values.

Norm	Δ,B,C,D	Conv-1D	X,Z	WikiText2	C4
				25.73	29.94
✓				24.76	29.02
	✓			23.27	27.22
		✓		25.24	29.09
			✓	24.99	28.88
✓	✓			22.51	27.00
✓		✓		24.93	28.87
✓			✓	25.31	29.43
	✓	✓		22.68	26.91
	✓		✓	22.97	26.41
		✓	✓	25.66	28.89
✓	✓	✓		**21.92**	**25.99**
✓	✓		✓	23.63	27,43
✓		✓	✓	24.89	29.04
	✓	✓	✓	23.01	26.98
✓	✓	✓	✓	23.73	28.19

Table 8: The performance of W16A16H4 quantization for Mamba2-370M with different trainable parameters in the ESR.

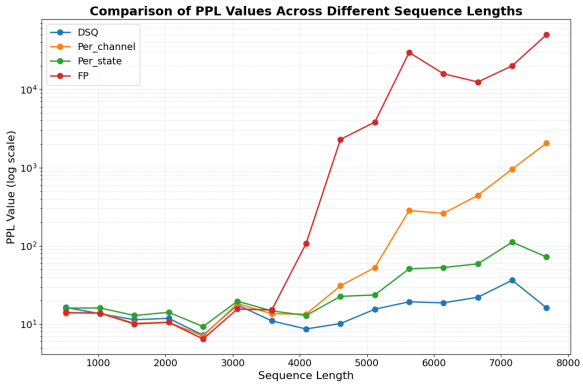

Figure 10: Illustration of perplexity with different length on PG-19 dataset.

A.5 Long Context Experiments

In Figure 10, we conducted additional evaluations on sequences longer than the 2048-token context reported in our main paper. We observed that the Mamba2-2.7B model suffers from significant performance degradation at a sequence length of 4K tokens. A similar phenomenon was previously reported in Stuffed Mamba (Chen et al., 2024b).

Surprisingly, however, we found that the quantized model maintains stable performance even at 8K tokens (Figure 10). We hypothesize that this discrepancy may be related to the state explosion problem described in Stuffed Mamba: "the explosion is largely contributed by a few dominant outlier channels. These outliers cause vanishing values in other channels when the output hidden representation is normalized." We hypothesize that quantization mitigates this issue by partially suppressing the impact of outlier channels. As illustrated in Figure 11, the state distribution of our quantized Mamba at 4k sequence length closely resembles that at 2k length.

A.6 More Detailed Latency Results

In Figure 6, we show the latency of Mamba2 models with different batch sizes. Here, we provide more detailed results regarding the latency of prefill and decoding stages.

Table 9: Latency (ms) for FP16 vs. W8A8H4 quantization.

Batch Size	Stage	FP16	W8A8H4
BS=32	Prefill	370	**239**
	Decoding	3734	**3208**
BS=64	Prefill	738	**509**
	Decoding	3786	**3472**

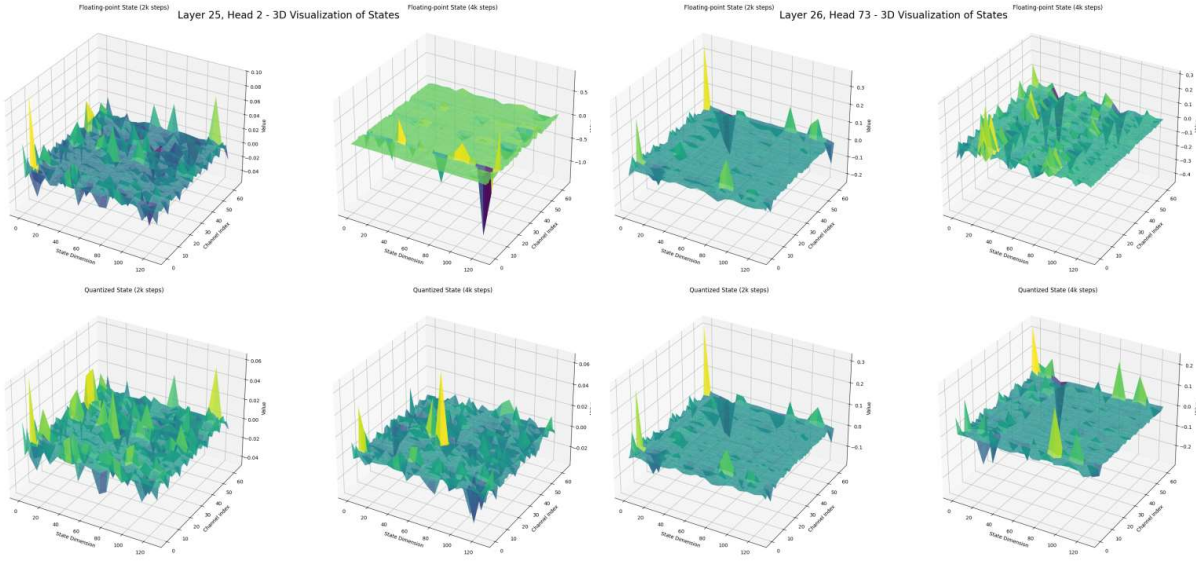

Figure 11: Visualization of .

A.7 Pseudocode

In this section, we present the pseudocode for the parallel training of quantization-aware SSMs. To enhance understanding, we also include the pseudocode for the recurrent and quadratic modes of Mamba-2. It is worth noting that these pseudocodes are provided solely for illustrative purposes and do not represent actual implementations.

```python
def ParallelSSM(
    A,  # bsz * num_head * len
    B,  # bsz * num_head * len * state_dim
    C,  # bsz * num_head * len * state_dim
    x  # bsz * num_head * len * channel_dim
):
    BC = C @ B.transpose(-1, -2)
    prefix_sum = torch.cumsum(A)

    # L : bsz * num_head * len * len
    L = torch.tril(prefix_sum.unsqueeze(-1) - prefix_sum.unsqueeze(-2))

    ABC = L * BC
    y = ABC @ x
    return y
```

```python
def RecurrentSSM_onestep(
    A,  # bsz * num_head
    B,  # bsz * num_head * state_dim
    C,  # bsz * num_head * state_dim
    x,  # bsz * num_head * channel_dim
    last_state  # bsz * num_head * channel_dim * state_dim
):
    current_state = A * last_state + B.unsqueeze(-2) * x.unsqueeze(-1)
    output = current_state @ C.unsqueeze(-1)
    return output.squeeze(-1)
```

```python
def QuantizationAwareParallelSSM(
    A,  # bsz * num_head * len
    B,  # bsz * num_head * len * state_dim
    C,  # bsz * num_head * len * state_dim
    x  # bsz * num_head * len * channel_dim
):
    BX = B.unsqueeze(-2) * x.unsqueeze(-1)
    prefix_sum = torch.cumsum(A)
    L = torch.tril(prefix_sum.unsqueeze(-1) - prefix_sum.unsqueeze(-2))
    state = torch.einsum('bhldn,bhll->bhldn', BX, L)

    # Simulate the quantization errors at the last timestep
    # Error case: qstate =  fake_quant(state)
    qstate = A[:, :, 1:] * fake_quant(state)[:, :, :-1] + BX[:, :, 1:]

    y = torch.einsum('bhldn,bhln->bhld', qstate, C)
    return y
```